MICROSTRUCTURE FORMATIONS IN THE TWO PHASE REGION OF THE BINARY PERITECTIC ORGANIC SYTEM TRIS-NPG

Johann Mogeritsch, Andreas Ludwig

University of Leoben, Department Metallurgy,
Franz-Josef-Strasse 18, 8200 Leoben, Austria

Keywords: Peritectic solidification, in-situ observations, microgravity

Abstract

In order to prepare for an onboard experiment on the International Space Station (ISS), systematic directional solidification experiments with transparent hypoperitectic alloys were carried out at different solidification rates around the critical velocity for morphological stability of both solid phases. The investigations were done in the peritectic region of the binary transparent organic TRIS-NPG system where the formation of layered structures is expected to occur. The transparent appearance of the liquid and solid phase enables real time observations of the dynamic of pattern formation during solidification. The investigations show that frequently occurring nucleation events govern the peritectic solidification morphology which occurs at the limit of morphological stability. As a consequence, banded structures lead to coupled growth even if the lateral growth is much faster compared to the growth in pulling direction.

Introduction

Experimental investigations under reduced gravity condition lead to a better understanding of the influence of gravitational related phenomena as natural convection and sedimentation on the solidification morphologies of peritectic alloys. For an alloy of peritectic composition the liquid [L], the primary solid [α] phase, and the peritectic [β] phase are in equilibrium at the peritectic temperature, T_p. The focus of the present investigation is put on the solidification morphologies at growth rates where one or both phases might reveal a planar solid/liquid interface. Such morphologies reveal a complex dynamic which is still not fully understood in detail.

Trivedi [1] published a conceptual model which predicts cyclic nucleation and overgrowth under purely diffusive growth conditions in the hypoperitectic region where both [α] and [β] phases would grow independently as planar fronts. Evidence for such bands were found in experiments where convection is suppressed by using thin samples [2,3]. Hunzinger et al. [4] developed a microstructure map with the nucleation and constitutional undercooling criterion under the assumption of infinitely high nuclei density and steady-state growth. Chalmers [5] predicted the simultaneous growth of both phases in form of lamellae or fibers and Lo et al. [6] show by simulation that bands are formed only for approximately equal volume fraction of the two phases otherwise islands are formed.

Directionally solidification experiments with metal alloys were carried out and published in [2, 3,7-17], but in-situ observations of peritectic solidification with transparent organic compounds were done recently only by the authors. Organic alloys with a high temperature non-faceted phase solidify in a metal-like manner and thus enable the detailed observation of the dynamic of the solid/liquid interface morphology during solidification. The transparent non-facetted/non-

facetted peritectic system TRIS–NPG [18,19] was selected for in-situ observations of solidification experiments with near peritectic compositions. The peritectic region of the TRIS-NPG phase diagram is shown in Fig. 1. Preliminary studies of the phase diagram show a thermal sensibility of the organic substance TRIS at temperatures close to the melting point which constrains the experimental process conditions. The diffusion coefficient in the liquid within the peritectic region could be measured as $D_L \approx 1.5 \cdot 10^{-11}$ m^2/s.

The observation was realized with a micro Bridgman-furnace and a light microscope in combination with a CCD camera. For the selected process conditions growth competition between the primary phase and the peritectic phase is expected and the growth of discrete bands are predicted [20-23]. Our experimental results show oscillatory and isothermal coupled growth morphologies within the peritectic region, published and discussed in details in [24-27].

In the present paper, we report the results of investigations for a hypoperitectic alloy with $x = 0.5$ mol fraction NPG at a fixed temperature gradient and variable solidification rates. Furthermore, the impact of different initial solid/liquid interfaces morphologies on the dynamic of peritectic solidification near the morphological stability limit of both phases was evaluated.

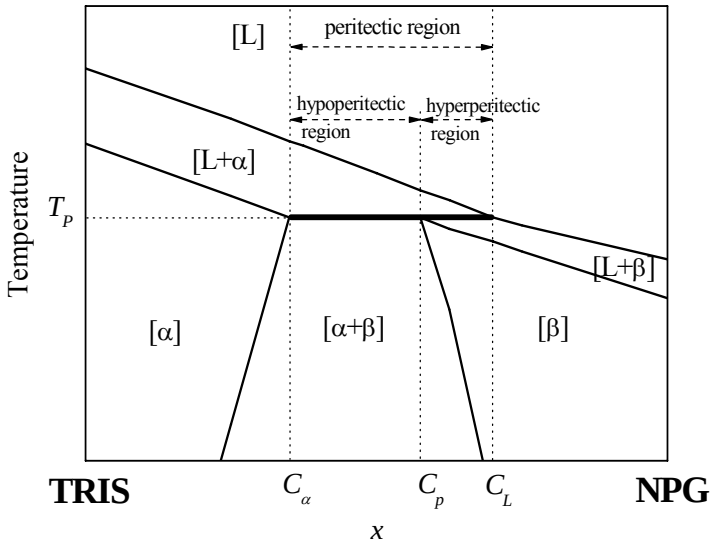

Figure 1. Detail of the TRIS –NPG phase diagram. At the peritectic temperature T_p and the peritectic concentration C_p the primary [α] phase, the peritectic [β] phase, and the liquid phase [L] are in equilibrium.

Experimental procedure

The organic substances TRIS and NPG were delivered as powder from Adrich [28] with an indicated purity of 99% and 99.9+%, respectively. Both substances are highly hydroscopic [29], whereby, the water content of the organic substance NPG was reduced by a drying process at 310 K for 24 hours. TRIS, sensitive to long time annealing and delivered with high-purity, was used without further purification. All operations were done in an argon atmosphere within a glove box.

The alloy preparation for the hypoperitectic concentration was done by mixing the powder of both organic substances in a glass container. Subsequently, the powder was heated up to the liquid state and cooling down to room temperature and storied for further use.

Extra large but thin rectangle glass samples (0.1 x 2.0 mm^2 inner dimensions with 100 µm wall thickness) were filled with liquid alloy by capillary force on a heater within the glove box. The sample itself has a length of more than 20 cm and 4 cm observation length can be used within the micro Bridgman-furnace. The movement of the glass sample through the furnace is PC-controlled which allows the application of different cooling rates.

The furnace itself consists of a heating and a cooling zone departed by a small adiabatic observation gap of 3.6 ± 0.1mm, see Fig. 2.

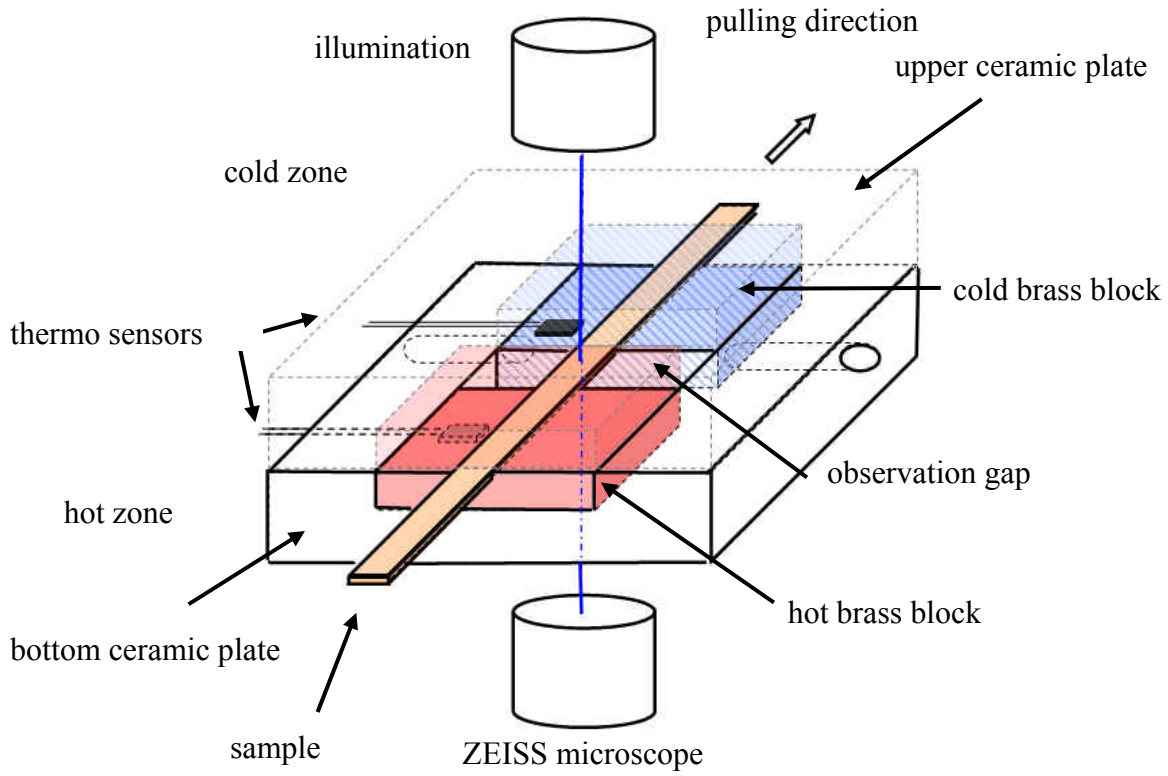

Figure 2: Sketch of the micro Bridgman-furnace.

The hot parts of the Bridgman-furnace are controlled by electrical resistant heaters and the cold parts are cooled by circulating water. The temperatures of the hot zone were measured with Pt 100 temperature sensors placed inside each brass block and regulated independently by a EUROTHERM 2408 controller [30] with an accuracy of ± 0.1 K. The temperature of the cold zone was measured with a Pt 100 temperature sensor placed between the brass blocks and regulated by a water cooling system with an accuracy of ± 0.5 K measured within the water tank of the pump. A slot of 0.4 x 2.5 mm^2 is milled in the hot and cold brass block of the bottom plate to host the sample.

The sample are illuminated from the top and observed from the bottom with the used ZEISS microscope. The construction of the Bridgman-furnace enables a field of view of 3180 x 2760 μm^2.

For the optical investigations, the microscope was equipped with a ½" Pulnix TMC-6700 digital camera with a resolution of 648 x 484 pixels. During solidification the taken images were recorded simultaneously with relevant temperatures from the furnace.

For the experiments, the micro Bridgman-furnace is preheated to bring the entire system, furnace and microscope, in a thermally equilibrated stage. After 1 hour the desired temperature gradient of $G_T = 14.5$ K/mm in the furnace is stable and a sample is placed into the furnace. The sample was held at least 30 minutes to prepare a planar solid/liquid interface. Now, the sample is ready for the solidification experiment and the optical system is started to record pictures and temperatures. Solidification experiments were carried out in two different ways: (i) at a constant pulling rate close to the constitutional undercooling limit with a corresponding concentration profile in front of the planar solid/liquid interface, or (ii) the sample was moved with a high pulling rate above the morphological stability limit (here $V_p = 115$ µm/s) for 30 seconds to create localized concentration fields around dendrites tips. Afterwards, the sample was moved with a pulling rate clearly below the morphological stability limit (here $V_p \leq 0.89$ µm/s) through the furnace.

Results and discussion

The investigations of a hypoperitectic alloy with $x = 0.5$ mol fraction NPG with solidification rates from 1.28 µm/s to 0.06 µm/s and two different initial solid/liquid interfaces show a wide range of solidification morphologies. We are able to observe simultaneous growth of [α] and [β] phases in form of an oscillating coupled growth and isothermal coupled growth. The results are published and discussed in [25, 27].

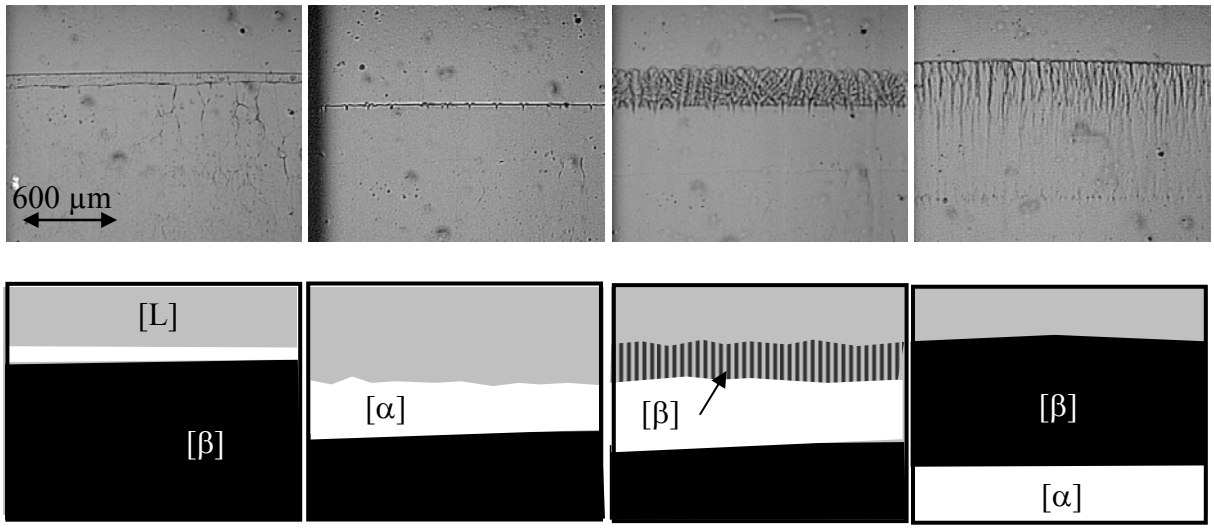

Figure 3. Development of layered solidification structure.

In some cases only the change from [α] planar growth to [β] planar growth or vice versa was observed. In other cases we found the formation of layers by the mechanism shown in Fig.3a-d.

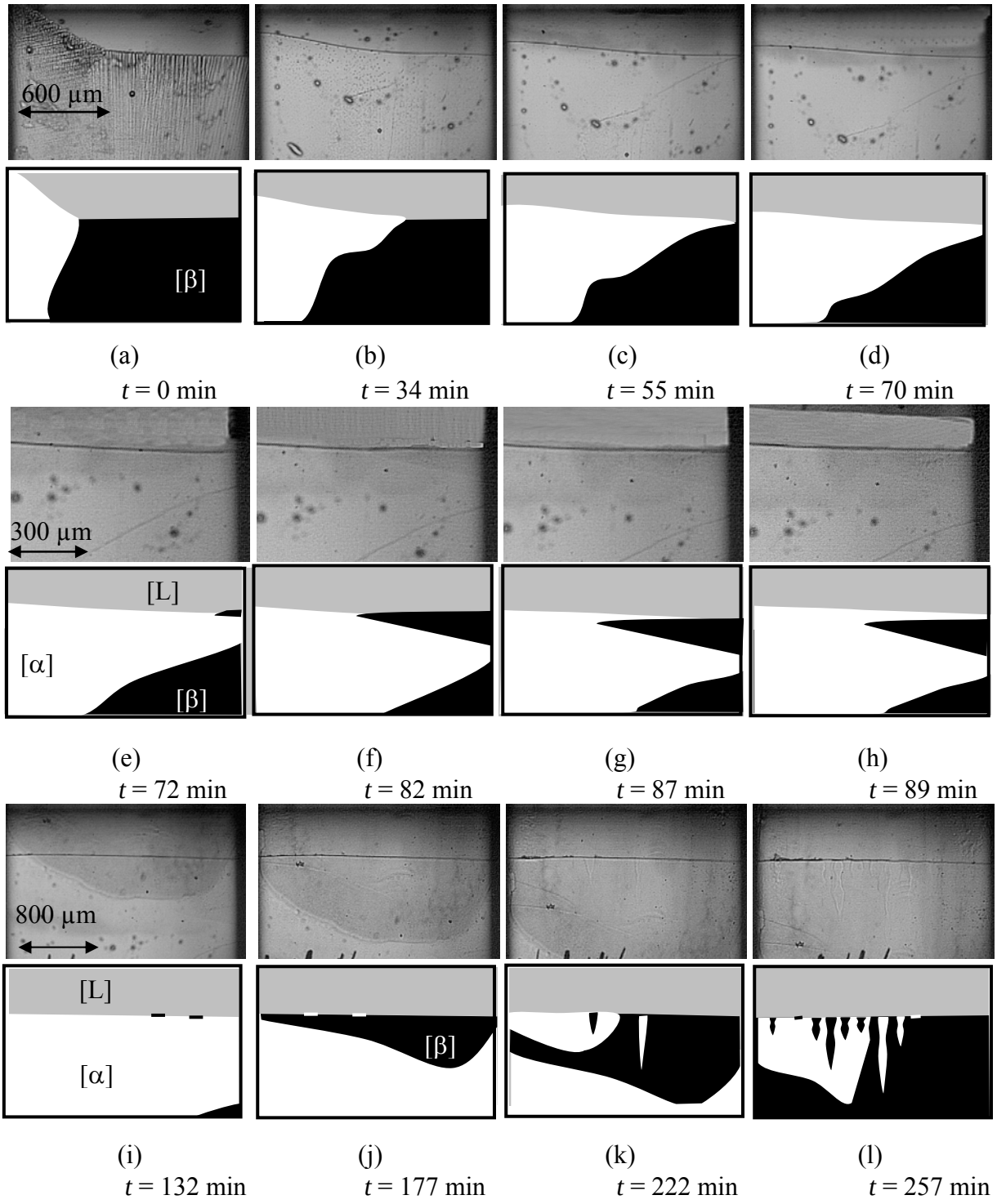

Figure 4. Evolution of the solidification morphology from a planar solid/liquid interface to an isothermal coupled growth. Note that the dark and bright grey shadows visible in Fig. 4i-k result from an uneven sample illumination.

Here, the solidification starts with a planar interface of the [β] phase and the formation of an [α] band along the solid/liquid interface (Fig. 3a). Now, the solid/liquid interface goes to a lower temperature and became unstable (Fig. 3b). In this moment, the [β] phase nucleates multiple on

the liquid/[α] interface and start to propagate as dendrites (Fig. 3c). As soon as the dendrite tips reach the solidus line of the [β] phase the solidification morphology transforms to a planar solid/liquid interface, see Fig. 3d. The cycle from Fig. 3b to Fig. 3d was observed 3 times with different time intervals in between.

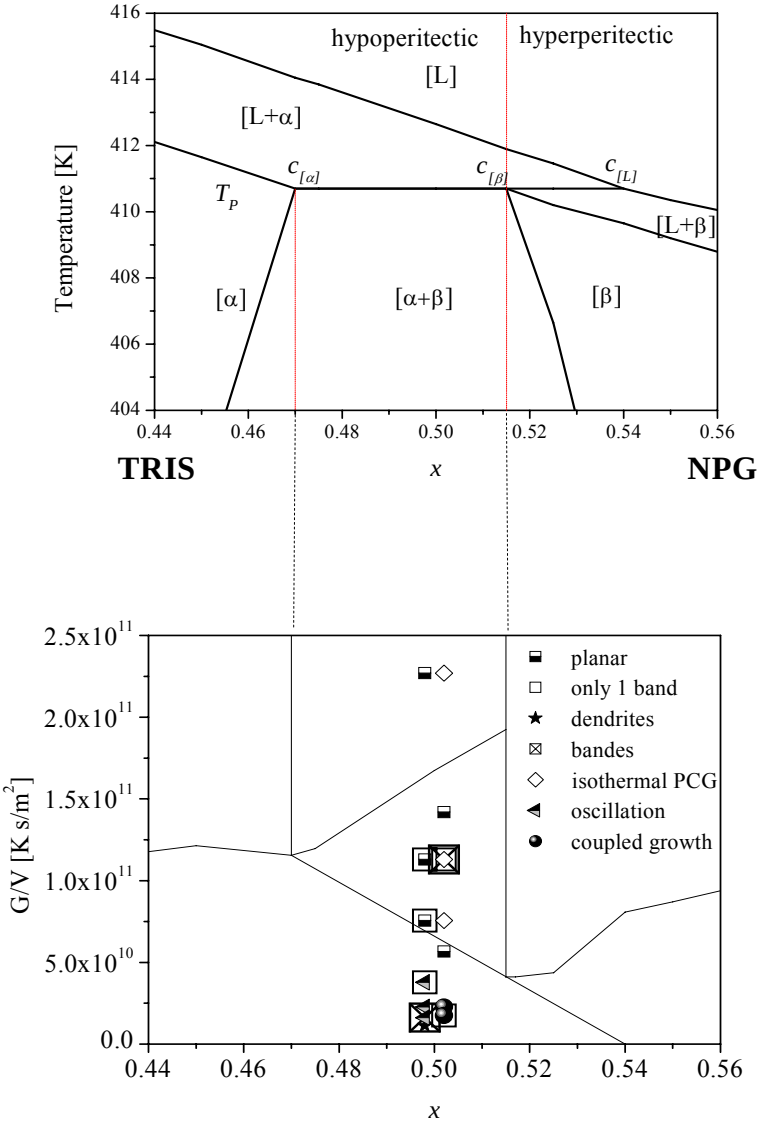

Figure 5: Peritectic region of the phase diagram and calculated microstructures depending on the applied *G/V* and the mol fraction *x* as full lines. The solidification morphologies for a hypoperitectic concentration are given as symbols. Experiments with a initial planar front are in the left column and results with a dendritic/cellular initial interface are on the right one.

Another form of layered solidification structures is shown in Fig. 4. Here, the initial solid/liquid interface is dendritic/cellular. During the fast movement of the sample the [α] phase nucleates on the wall or on the wall-solid-liquid junction, see Fig 4a. Following this, the pulling rate is changed from fast movement with V_p = 115 µm/s to a slow movement with V_p = 0.13 µm/s.

Within the first 10 minutes the interface changes into a planar solidification morphology. The [α] phase, visible on the left corner of the picture in Fig. 4a, grows laterally with $V_\alpha = 0.34 \pm 0.05$ µm/s along the solid/liquid interface of the [β] phase, see Fig. 4a-c. The entire [β] phase is overgrown in Fig. 4d and only the [α] phase grows further on. After the growth of an [α] phase band of 133 ± 22 µm the [β] phase nucleates on the solid/liquid/wall junction and starts to grow from the right side to the left side of the sample with $V_\beta = 1.11 \pm 0.1$ µm/s (see Fig. 4e-f). Whereby, the [β] phase is overgrown by the [α] phase, with $V_\alpha = 0.69 \pm 0.1$ µm, before the [β] phase reaches the other side of the sample, as visible in Fig. 4g-h. Only a section with a maximum wide of 166 ± 22 µm is created. The [α] phase grows stable for further 200 ± 22 µm before the [β] phase nucleates again. Now, nucleation takes place on the solid/liquid interface with a distance between the nucleation events of 500 ± 120 µm (Fig. 4i). The [β] phase overgrows with $V_\beta = 0.46 \pm 0.05$ µm the [α] phase along the entire solid/liquid length and creates a new [β] phase band with a maximum of 535 ± 20 µm and a minimum of 20 µm. Further on, the [α] phase nucleates at the solid/liquid interface of the [β] phase (Fig. 4j) and starts to grow laterally with $V_\alpha = 0.51 \pm 0.05$ µm. Before the [α] phase overgrows the [β] phase multiple nucleation events happen on the solid/liquid interface (Fig. 4k). The distance between the nucleation events is now gradually reduced and the solidification morphology changes to isothermal coupled growth.

It is important to notice that all lateral growth velocities are faster than the solidification velocity in pulling direction. Further more, the small thickness of the sample suppresses convection. Nevertheless, only parts of bands were grown. Instead, the layered structure of bands changes to isothermal peritectic coupled growth [22]. It seems that in the present NPG-TRIS system nucleation dominates against lateral growth. The results of our investigations for a hypoperitectic concentration with $x = 0.5$ are gathered in the microstructure map shown in Fig. 5. For a better visualization experiments with an initial planar front are put on the left side and the ones with an initial dendritic/cellular interface are put on the right side.

Conclusions

We have investigated the relationship between solidification velocity and the solid/liquid interface morphology during solidification of an alloy of hypoperitectic composition at $x = 0.5$. Experiments were carried out in a micro Bridgman-furnace at different solidification rates and a constant temperature gradient. For pulling rates above the morphology stability limit of both solid phases we found an oscillatory solidification dynamic of dendritic/cellular kind [25]. For pulling rates below these limits we observed (i) a change of planar growth from on to the other solid phase, (ii) isothermal coupled growth, and (iii) lateral bands which finally also turn into isothermal coupled growth. The results show no significant dependence on whether the initial solid/liquid interface was planar or dendritic/cellular. Although we found that the lateral growth of the respective other phase is much faster than the forwards solidification rate, multiple nucleation promote the formation of isothermal couple growth.

Acknowledgements

This work was supported in part by the European Space Agency ESA and in part by the Austrian Space Agency ASA through means of the ESA map project METCOMP.

References

[1] R. Trivedi, *Metall. Mater. Trans.,* 26A (1995) 583-90.
[2] J.S. Park, R. Trivedi, *J. Cryst. Growth*, (1998) pp. 511.
[3] H. Yasuda, I. Ohnaka, K. Tokieda, Solidification processing. University of Sheffield 1997, 44-8.
[4] O. Hunziker, M. Vandyoussefi, W. Kurz, *Acta Mater*, 46 (1998) 6325-36.
[5] B. Chalmers, *Physical Metallurgy,* New York Wiley (1959)
[6] T.S. Lo, A. Karma, M. Plapp, *Phys Rev E*, 63 (2001) pp. 031504.
[7] Y. Li, S.C. Ng, H. Jones, *Scripta Mater.,* 39 (1998) 7-11.
[8] P. Busse, F. Meissen, *Scripta Mater.*, 36 (1997) 653-8.
[9] L.S. Luo, Y.Q. Su, J.J. Guo, X.Z. Li, S.M. Li, H. Zhong, L. Liu, H.Z. Fu, *J. Alloys Comp.*, 461 (2008) 121-7.
[10] Y.Q. Su, L.S. Luo, X.Z. Li, J.J. Guo, H.M. Yang, H.Z. Fu, *Appl. Phys. Lett.*, 89 (2006) 2319181-3.
[11] L.S. Luo, Y.Q. Su, X.Z. Li, J.J. Guo, H.M. Yang, H.Z. Fu, *Appl. Phys. Lett.*, 92, (2008) 0619031-3.
[12] T.S. Lo, S. Dobler, M. Plapp, A. Karma, W. Kurz, *Acta Mater.*, 51 (2003) 599-611.
[13] S. Dobler, T.S. Lo, M. Plapp, A. Karma, W. Kurz, *Acta Mater.*, 52 (2004) 2795-808.
[14] J.H. Lee, J.D. Verhoeven, *J. Cryst. Growth*, 144 (1994) 353-66.
[15] H.W. Kerr, W.Kurz, *Int. Mater. Rev.*, 41 (1996) 129-64.
[16] W.Luo, J.Shen, Z.Min, H.Fu, *J. Cryst. Growth*, 24 (2008) 5441-6.
[17] W.Z. Luo, J. Shen, Z.X. Min, H.Z. Fu, *Mater. Lett.*, 63 (2009) 1419-21.
[18] L. Sturz, V.T. Witusiewicz, U. Hecht, S.Rex, *J. Crystal Growth*, 270 (2004) 273-82.
[19] M. Barrio, D.O. Lopez, J.L. Tamarit, P. Negrier, Y .Haget, *J. Solid State Chem.*, 124 (1996) 29-38.
[20] W.J. Boettinger, *Metall.Trans.*, 5 (1974) 2023-31.
[21] R. Trivedi, J.S. Park, *J. Cryst. Growth*, 235 (2002) 572-88.
[22] F. Kohler, L. Germond, J.D. Wagniére, M.Rappaz, *Acta mater,* 57 (2009) 56-68.
[23] R. Trivedi, *Scripta Mat.*53 (2005) 47-52.
[24] J. Mogeritsch, A. Ludwig, S. Eck, M. Grasser, B. McKay, *Scripta Mater.*, 60 (2009) 882-5.
[25] A. Ludwig, J. Mogeritsch, M. Grasser, *Trans. Indian Inst. Met.*, 62 (2009), 433-6
[26] J. Mogeritsch, S. Eck, M. Grasser, A. Ludwig, *Mater. Sci. Forum*, 649 (2009) 159-64.
[27] J. Mogeritsch, A. Ludwig, John Hunt International Symposium, London (2011), in print.
[28] http://www.sigmaaldrich.com (access date: 30.10.2011).
[29] NPG CAS-No 126-30-7 and TRIS CAS-No 77-86-1.
[30] http://www.eurotherm.com (access date: 30.10.2011).